PCCP

Accepted Manuscript

ROYAL SOCIETY OF CHEMISTRY

www.rsc.org/pccp

PCCP

RSCPublishing

COMMUNICATION

Exploring few-layer graphene and graphene oxide as fillers to enhance the oxygen-atom corrosion resistance of composites

Cite this: DOI: 10.1039/xoxxoooooox

Min Yi,[ab] Zhigang Shen,*[abc] Xiaohu Zhao,[b] Lei Liu,[ac] Shuaishuai Liang[a] and Xiaojing Zhang[a]

Received ooth January 2012,
Accepted ooth January 2012

DOI: 10.1039/xoxxoooooox

www.rsc.org/

Few-layer graphene (FLG) and graphene oxide (GO) were explored to enhance the oxygen-atom corrosion resistance of composites. FLG flakes of two different average lateral sizes (large: ~1.3 μm^2 and small: ~0.23 μm^2) were prepared by a centrifugation-based size selection route. After exposed in oxygen atom, though all fillers could enhance the oxygen-atom corrosion resistance of the composites, we found much greater enhancement by using large FLG, i.e. adding 1 wt% large FLG can achieve 42% decrease in the composites' mass loss. Bonding and barrier effects of the flaked fillers are responsible for the enhanced resistance. These preliminary, yet intriguing results pave a novel way for resisting oxygen-atom corrosion.

Graphene has been widely investigated in both fundamental aspects and potential applications across a great many fields.[1-4] It has been acknowledged that apart from the unique combination of strength, ductility, and conductivity, graphene has other exceptional physical and chemical properties. Firstly, graphene possesses excellent barrier properties. For example, graphene has even been used to create an air-tight ''balloon'' which shows impermeability to oxygen.[5] Secondly, graphene has remarkable inertness to oxidizing gas and liquid solutions,[6] being inert under conditions where other substances would undergo rapid chemical reactions. These exceptional properties make graphene uniquely suitable as an anticorrosion material. Therefore, research into graphene as an anticorrosion material is now rapidly flourished.

Recently, Chen *et al*. demonstrated that chemical vapour deposition (CVD) graphene coatings can protect Cu and Cu/Ni alloy from corrosion in air and hydrogen peroxide.[6] Prasai *et al*.,[7] Raman *et al*.,[8] and Kirkland *et al*.[9] showed that CVD graphene coatings can increase the resistance of metals to electrochemical corrosion. Also, Chang *et al*. reported polyaniline/graphene composites as coatings for corrosion protection of steel.[10] Kousalya *et al*. studied graphene as an oxidation barrier coating for liquid and liquid-vapour phase-change cooling systems.[11] However, these investigations are all focused on graphene as anticorrosion coatings, are mainly within the scope of CVD graphene, and are restricted to common corrosion induced by water, electrochemistry, and corrosive solutions. The study and application of graphene in corrosion fields are highly recommended to be further extended.

Herein, we extend the potential application to corrosion induced by oxygen atom. Presently, most studies lack coverage of the topic on using graphene in oxygen-atom corrosion filed. In oxygen atom, the presence of two unpaired electrons gives ^{3}p oxygen two reactive sites that are used to form bounds with other atoms or molecules, especially the hydrogen-containing molecules and the molecules that have no unpaired electron. In general, oxygen atom can easily oxidize polymers which are often not oxidized by molecular oxygen in ambient environment for a long time. Here, oxygen-atom corrosion means that the highly oxidative oxygen atom can violently react with polymer chains and thus result in heavy and quick corrosion of polymer surface. Even in the dry or vacuum environment, for example in the low earth orbit, a very small amount of oxygen atom can easily corrode the polymer heavily. One potential application of this topic is enhancing the oxygen-atom corrosion resistance of the spacecraft polymeric parts in the low earth orbit where oxygen atom exists and corrosion induced by space environment has huge danger. Following the similar idea of CVD graphene as a protection layer, we can anticipate that the use of CVD graphene for oxygen-atom-resistant layer is more straightforward. Nevertheless, we leave this route to be studied in the near further. As a compromise, considering that presently liquid-exfoliated few-layer graphene (FLG) can be easily produced in large scale and the industrial application in spacecraft may need scalable FLG, we try to use liquid-exfoliated FLG and explore the potential for FLG and graphene oxide (GO) as fillers to enhance the oxygen-atom

corrosion resistance of polymers. To date, the ability of FLG and GO as fillers to improve the oxygen-atom corrosion resistance in a functional context has not been extensively pursued. It can be anticipated that FLG and GO as fillers to enhance the oxygen-atom corrosion resistance of polymers may advance their application fields.

Polyvinylalcohol (PVA) was chosen to form composites with FLG and GO flakes as fillers. Though PVA is not a typical material for industrial application in corrosion field, many researchers have demonstrated it as an excellent matrix to study reinforced polymers and thought it as an excellent model polymer to study graphene or GO composites.[12-14] Therefore, as a fundamental research here, we choose PVA as a model polymer to study oxygen-atom corrosion. In order to prepare composites, we firstly prepared PVA/FLG dispersions by sonication and centrifugation and prepared GO dispersions by Hummers method and sonication (see ESI† for detail). With PVA as stabilizer, FLG flakes can be stabilized in water to form homogeneous colloid, as shown in Fig. 1a. The UV-vis spectrum in Fig. 1b is featureless in the visible region, as expected for a quasi-two-dimensional material.[15] The absorption peak of the FLG dispersion occurs at ~270 nm (Fig. 1b), suggesting that the electronic conjugation within the FLG flakes is retained.[16]

Following the idea that graphene flakes size has a critical role on the properties of graphene reinforced composites, we adopted controlled centrifugation to select FLG flakes with larger lateral size.[12, 17] Firstly, we used 2000rpm (×1024g) to obtain ~0.27 mg/mL FLG dispersions which contain small FLG flakes, as shown in Fig. 1d and Fig. S1c and d (see ESI†). Then we collected the sediment and diluted it by PVA solution. The diluted dispersions were further sonicated and centrifuged at a low rotation speed of 500rpm (×64g). The resultant dispersions have a FLG concentration of ~0.8 mg/mL. These dispersions contain large FLG flakes, as shown in Fig. 1c and Fig. S1a and b (see ESI†). Based on the atomic force microscopy (AFM) analyses, it can be seen that both the large FLG flakes (Fig. 1c and Fig. S1a and b) and the small FLG flakes (Fig. 1c and Fig. S1c and d) have thickness of ~1-1.2 nm. This thickness size confirms the high degree of exfoliation and thus the FLG flakes' high quality. These several atomic-layered flakes also ensure the large aspect ratio which has been deemed as an important parameter in reinforcing composites. Through statistical analysis of AFM images, we can quantitatively know the lateral size of the FLG flakes, as shown in Fig. 1f. The small FLG flakes before size selection have an average area of <A> ~0.23 μm^2, while the large FLG flakes achieved by size selection are of much larger area, with <A> ~1.3 μm^2. This statistical analysis confirms the effectiveness of selecting FLG lateral size by centrifugation.

We also performed Raman spectra on the vacuum filtered films of these FLG flakes (Fig. 1g). Both the 2D bands show the nature of FLG.[18] I_D/I_G, D/G band ratio which is a measure of defect content, is ~0.07 and ~0.22 for the large and small flakes, respectively. Defects in graphene can be basal plane defects or edge defects. Seeing that the G bands are not notably widened, the basal plane defect content should be very small.[19]

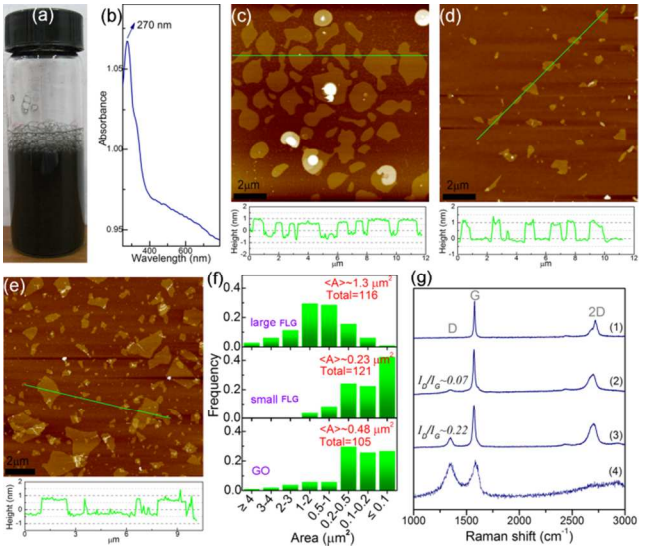

Fig. 1 (a) Photograph of PVA/FLG dispersions after 500rpm (×64g) centrifugation. (b) UV-vis spectrum of PVA/FLG dispersions in (a) diluted by 30. (c) Typical AFM image of large (size selected) FLG flakes after centrifugation of 500rpm. (d) Typical AFM image of small FLG flakes after centrifugation of 2000rpm. (e) Typical AFM image of GO. (f) Histograms for flake area of GO, small FLG, and size-selected large FLG. (g) Raman spectra of (1) pristine graphite and vacuum filtered films of (2) large FLG and (3) as-prepared small FLG, and (4) GO.

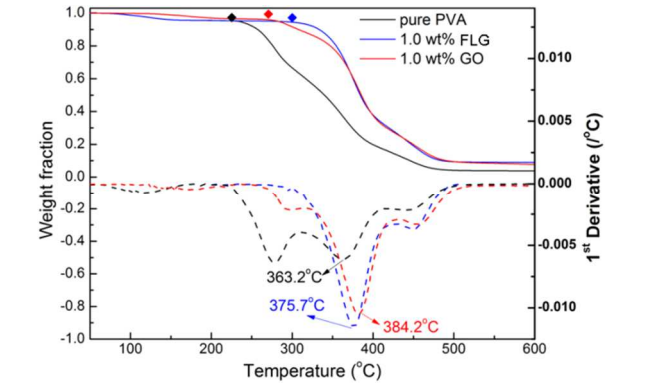

Fig. 2 TGA curves and the corresponding DTG curves of pure PVA, PVA composite with 1.0 wt% loading of large FLG, and 1.0 wt% GO/PVA composite.

The edge defects are unavoidable in the flaked FLG here. However, I_D/I_G in large FLG is much lower than that in small FLG. This is consistent with the results on lateral size, because I_D/I_G is inverse proportional to the mean flake length[20-21] and small flakes have much more edges per unit mass so that increase the content of edge defects.

GO was also prepared to form composites with PVA. As shown in Fig. 1e, GO flakes are ~1-nm thick and ~0.48-μm^2 large, but the unselected lateral size is widely distributed and many wrinkles appear. Raman spectrum of GO also indicates high-concentration defects ((4) in Fig. 1g).

Free standing composite films were prepared by solution casting of these PVA/FLG and PVA/GO composite dispersions (see ESI† for details). We firstly studied the thermal stability of

these films. Fig. 2 gives the thermogravimetric analysis (TGA) and corresponding differential thermogravimetric analysis (DTG) results for pure PVA and its composites. The TGA curves of the composites are shifted toward a higher temperature when compared to that of pure PVA. By adding only 1.0 wt% FLG or GO, the onset decomposition temperature is substantially increased by ~45-75 ^{o}C. Also the maximum temperature, which is defined as the peak on the derivation of the TGA curve, is enhanced by ~12-21 ^{o}C. Several reasons may account for the enhancement in thermal stability. Firstly, the higher thermal conductivity of FLG or GO can facilitate heat dissipation within the composites.[22-23] Secondly, as two dimensional material with high surface area, FLG or GO flakes can interact with more PVA chains,[23] resulting in much slower degradation of PVA chains at the matrix-filler interface. Thirdly, with extremely large aspect-ratio, the flaked FLG or GO layers can act as superior barriers to hinder the flux of volatile degradation products and thereby delay the degradation.[23]

As shown in Fig. S2 (see ESI†), the enhancement in mechanical properties also indicates strong interactions between the fillers and PVA matrix. We further conducted scanning electron microscopy (SEM) on the fractured surface (broken by tension) of composites to test the dispersed state of the filled flakes in the matrix. As shown in Fig. 3a and b, in contrast to the featureless and smooth fractured surface in pure PVA, in the fractured surface of 1.0 wt% FLG/PVA composite a large number of FLG flakes can be seen protruding. These protruded flakes are well dispersed and evenly distributed. Most importantly, these flakes protrude parallel to the tensile direction, suggesting the flakes to be aligned in the plane of the composite film. This in-plane alignment is attributed to the solution cast method, which has been previously evidenced in other composites and films.[12, 24-25] It should be noted that the flakes' in-plane alignment will help to form much better barriers to oxygen-atom penetration.

Oxygen-atom exposure was carried out in a ground-based atom oxygen effect simulation facility (see ESI† for details).[26-27] The accumulative atomic oxygen flux was about 4.7×10^{20} atoms/cm^2. Shown in Fig. 3d-f are the SEM images of the oxygen-atom corroded surface of pure PVA and composite films. Apparently, the surface morphology after oxygen-atom exposure is greatly distinct. The pure PVA film surface is severely corroded and roughened, exhibiting "carpet-like" structures with deep caves (Fig. 3d). The surface oxygen content is also highly increased as presented in X-Ray photoelectron spectrometer (XPS) results in Fig. 3g. In contrast, the surfaces of the composite films are smoother and less heavily corroded, with flaked fillers exposed after PVA matrix is corroded away (Fig. 3e and f). However, the morphology in GO reinforced and FLG reinforced composites is intrinsically different. As shown in Fig. 3f, "carpet-like" structures still appear on the surface of PVA/GO film, though they are less notable. In addition, only few GO flakes are retained on the corroded surface and the retained GO flakes are fluffy and wrinkled. In contrast, the corroded surface of PVA/FLG composite (Fig. 3e) is much smoother and almost shows no "carpet-like" structures. Lots of FLG flakes still remain on the corroded surface. The XPS survey also evidences that the

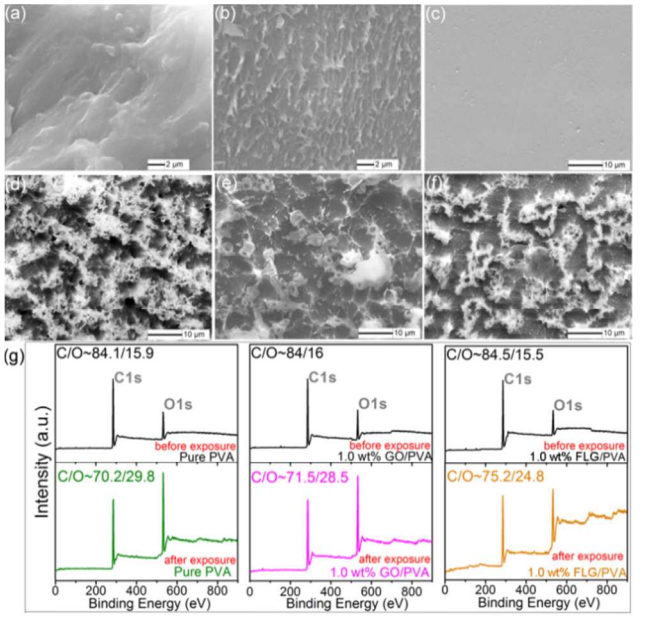

Fig. 3 SEM images of tension-fractured surfaces of (a) pure PVA film and (b) 1.0 wt% large-FLG/PVA film. (c) Surface SEM image of pure PVA film before oxygen-atom exposure. Surface SEM images of (d) pure PVA film, (e) 1.0 wt% large-FLG/PVA film, and (f) 1.0 wt% GO/PVA composite film after exposed in a total oxygen-atom flux of ~4.7×10^{20} atoms/cm^2. (g) XPS survey of the surfaces of pure PVA, GO/PVA composite, and large-FLG/PVA composite before and after oxygen-atom exposure.

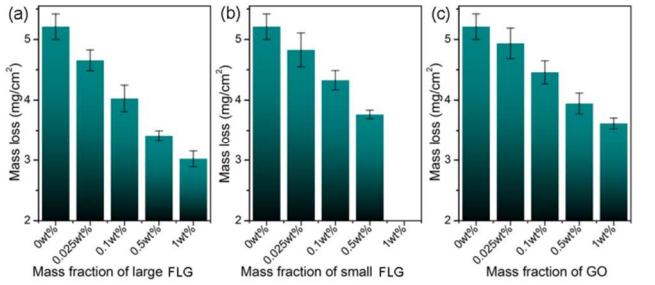

Fig. 4 Mass loss of composite films with different loading of (a) large FLG flakes, (b) small FLG flakes, and (c) GO flakes after exposed into oxygen atom. The total oxygen-atom flux (~4.7×10^{20} atoms/cm^2).

surface carbon content is much higher in large-FLG/PVA film (Fig. 3g). This indicates much more FLG flakes retained after oxygen-atom exposure. This morphology difference and XPS survey results indicate that FLG flakes and GO flakes may have different effects on oxygen-atom corrosion resistance. FLG flakes may be more favourable for enhancing resistance of polymers to oxygen atom. This speculation will be further evidenced and discussed in the following.

Besides the above distinct morphology, the mass loss has been the critical parameter for quantitatively assessing the oxygen-atom corrosion resistance of a material. We have plotted the mass loss as a function of the fillers' loading, as shown in Fig. 4. Obviously, after embedment of these flaked

fillers, the mass loss of PVA decreases. Importantly, an addition of 0.5 wt% large FLG (Fig. 4a), small FLG (Fig. 4b), and GO (Fig. 4c) can achieve ~34.5, ~27.7, and 24.2% decreases in mass loss, respectively. Only 1 wt% large FLG could result in a mass loss reduction of ~42%. We also tried higher filler loading, but the reduction in mass loss is less remarkable, possibly due to aggregations. For comparison, we have also added pristine graphite powder to reinforce PVA, but to find that 1 wt% graphite could result in a high mass loss reduction of ~ 4.7 mg/cm^2 (Fig. S3 in ESI†), even higher than that in the case of 0.1 wt% FLG loading. Therefore, in accordance with the results by examining morphology, the reduction in mass loss also exactly indicates that FLG and GO fillers can improve the oxygen-atom corrosion resistance of polymeric composites. These results in mass loss reduction are very attractive when compared to that by adding conventional fillers. For example, ~5 wt% nano SiO_2 can only lead to a reduction of ~42% in mass loss[28] and an extremely high loading of plerospheres (~50 wt%) can only lead to a reduction of ~68% in mass loss[29]. In this aspect, it has significant advantages that FLG and GO fillers with these very low loadings can match or even exceed the performance of large quantities of traditional fillers in improving oxygen-atom corrosion resistance.

Despite of the above verified enhanced resistance, the mass loss reduction by adding small FLG flakes (average ~0.23 μm^2) is comparable to or even more than that by adding larger GO flakes (average ~0.48 μm^2), as shown in Fig. 4b and c. Larger FLG flakes (average ~1.3 μm^2) can even result in much more reduction in mass loss. These quantitative results agree well with the above observed distinction in surface morphology (Fig. 3e and f), further indicating that FLG performs better than GO. We attribute this distinct performance to not only the mechanism that how flaked fillers enhance oxygen-atom corrosion resistance, but also the structure difference between graphene and GO.

As shown in Fig. 5a, two effects may contribute to the mechanism. The first is bonding effect, i.e. these flaked fillers with large surface area can react with oxygen atom to form bonds, thus consuming large quantities of oxygen atom. The second is barrier effect, i.e. these flaked fillers have barrier effects for oxygen-atom penetration and protect PVA matrix underneath from corrosion. However, large FLG flakes, small FLG flakes, and GO flakes have different performance in these two effects. FLG flakes can react with oxygen atom to form stable epoxy groups.[30-32] This can resist subsequent corrosion and alleviate PVA matrix corrosion by consuming abundant oxygen atom. This can be indirectly evidenced by that FLG flakes are not corroded away and still remain on the corroded surface (Fig. 3e). FLG flakes are also impermeable to standard gases including helium,[33-34] forming effective barrier for oxygen-atom penetration. Exactly, simulation work shows that the energy barrier for an oxygen atom passing from the top to the bottom side of monolayer graphene is as high as 5.98-16.34 eV and FLG with more layers will pose higher energy barrier.[35] This energy barrier is higher than the typical energy (4-5 eV) of oxygen atom in LEO environment.[26] So FLG flakes could protect PVA underneath from oxygen-atom corrosion through barrier effects. Meanwhile, as shown in Fig. 5b and c, larger FLG flakes have much fewer edges and allow much less penetrative channels than smaller ones, resulting in much better

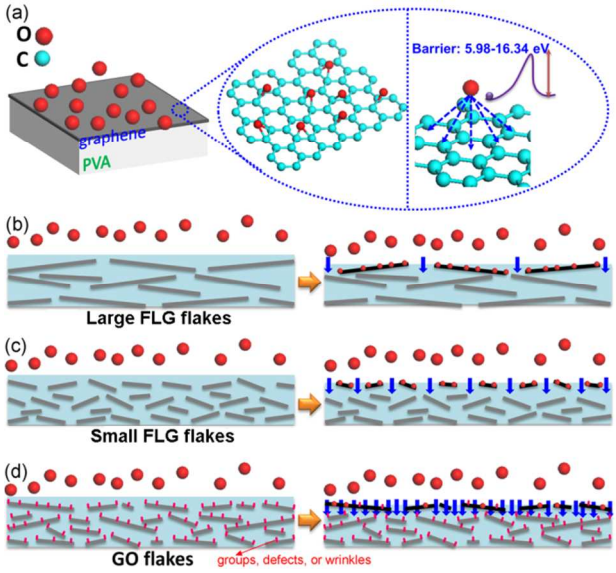

Fig. 5 Schematic of the mechanism that FLG and GO flakes can enhance oxygen-atom corrosion resistance of PVA composites. (a) Two possible routes for the mechanism. (b) Large FLG flakes allow less penetrative channels. (c) Small FLG flakes allow more penetrative channels. (d) GO flakes allow much more penetrative channels due to the violent reaction between oxygen atom and the attached groups, defects, and wrinkles.

barrier effects. In contrast, GO flakes suffer from severe defects, numerous groups, and many wrinkles (Fig. 1e and g). Carbon atoms within these defects, groups, and wrinkles often show enhanced reactivity and could react with oxygen atom violently.[36-37] This can lead to GO flakes spilt into cracked fragments and thus much weaker barrier effects,[38-40] as illustrated in Fig. 5d. These cracked GO fragments may be eventually corroded away, as indirectly evidenced by that GO flakes are rarely observed in the corroded surface (Fig. 3f) and that the surface carbon content is similar to that in pure PVA after exposure (Fig. 3g). Therefore, in GO flakes, the highly defected and wrinkled structures with high reactivity and thus much weaker barrier effects are accountable for the inferior performance.

Another two factors, i.e. flake edges and cutting effects, which weaken the barrier effects, must be mentioned. As an ideal or perfect infinite FLG flake (i.e. no edges or defects), no oxygen atom could penetrate through it,[30, 35] FLG can act as perfect coatings for preventing oxygen-atom corrosion,[30, 35] and no mass loss would appear in PVA composites. However, the FLG here is flaked, with many edges though no severe defects in basal plane. Oxygen atom could react with theses reactive edges[41] and gradually corrode away carbon atoms from the edges.[42] In addition, oxygen atom has cutting effects on both FLG and GO flakes,[38-40] but GO flakes with pre-existed numerous epoxy groups in the basal plane are much more easily cut into pieces than FLG flakes when exposed into the same

amount of oxygen atom; because the aligned epoxy groups in GO are the preferable positions for the cutting process during further oxidation.[38-40] These two factors progressively make FLG smaller but make GO flakes rapidly cut into pieces, thus weakening the barrier effects, as schematized in Fig. 5b-d. This is the possible reason why mass loss reduction (~42%) by adding FLG flaked filler (1 wt%) is not so amazing as expected. The design of large-area graphene and in-plane aligned homogeneous dispersion to further enhance the performance in resisting oxygen-atom corrosion of composites should be continued in the near further.

Conclusions

In conclusion, we have explored the potential of FLG and GO as fillers to enhance the oxygen-atom corrosion of polymeric composites. By sonication and centrifugation-based size selection, we prepared FLG/PVA hybrid dispersions with FLG flakes of two different averaged area, ~1.3 μm^2 (large FLG) and ~0.23 μm^2 (small FLG). GO flakes are of widely distributed lateral size, with an averaged area of ~0.48 μm^2. These composites show high enhancement in thermal stability. All these flaked fillers can enhance oxygen-atom corrosion resistance. Large FLG performs much better than small FLG and GO. Adding only 1 wt% large FLG can achieve 42% decrease in composites' mass loss. It is suggested that bonding and barrier effects of the flakes are responsible for the enhanced resistance. Large-surface-area flakes can react with oxygen atom to form bonds, thus consuming abundant oxygen atom. FLG has much better barrier effects than GO, hence leading to much higher resistance to oxygen atom. We hope that these preliminary, yet intriguing results could establish FLG and GO as the vigorous functional materials available for resisting oxygen-atom corrosion.

Acknowledgements

The authors acknowledge the financial support by the Beijing Natural Science Foundation (2132025), Specialized Research Fund for the Doctoral Program of Higher Education (20131102110016), Special Funds for Co-construction Project of Beijing Municipal Commission of Education, Innovation Foundation of BUAA for Ph.D. Graduates, and Innovative Practice Foundation of BUAA for Graduates (YCSJ01201309).

Notes and references

[a] *Beijing Key Lab. for Powder Technology Research and Development, Beijing University of Aeronautics and Astronautics, Beijing 100191, China.*
[b] *Plasma Lab., Ministry-of-Education Key Lab. of Fluid Mechanics, Beijing University of Aeronautics and Astronautics, Beijing 100191, China.*
[c] *School of Material Science and Engineering, Beijing University of Aeronautics and Astronautics, Beijing 100191, China.*
Fax:+ 86 10-82338794; Tel: +86 10-82317516; E-mail: shenzhg@buaa.edu.cn

† Electronic Supplementary Information (ESI) available: experimental details, additional AFM and SEM images. See DOI: 10.1039/x000000x/

1. A. K. Geim and K. S. Novoselov, *Nat. Mater.*, 2007, **6**, 183.
2. L. P. Biro, P. Nemes-Incze and P. Lambin, *Nanoscale*, 2012, **4**, 1824.
3. K. S. Novoselov, V. I. Fal'ko, L. Colombo, P. R. Gellert, M. G. Schwab and K. Kim, *Nature*, 2012, **490**, 192.
4. R. Mas-Balleste, C. Gomez-Navarro, J. Gomez-Herrero and F. Zamora, *Nanoscale*, 2011, **3**, 20.
5. J. S. Bunch, S. S. Verbridge, J. S. Alden, A. M. van der Zande, J. M. Parpia, H. G. Craighead and P. L. McEuen, *Nano Lett.*, 2008, **8**, 2458.
6. S. Chen, L. Brown, M. Levendorf, W. Cai, S. Y. Ju, J. Edgeworth, X. Li, C. W. Magnuson, A. Velamakanni, R. D. Piner, J. Kang, J. Park and R. S. Ruoff, *ACS Nano*, 2011, **5**, 1321.
7. D. Prasai, J. C. Tuberquia, R. R. Harl, G. K. Jennings, B. R. Rogers and K. I. Bolotin, *ACS Nano*, 2012, **6**, 1102.
8. R. K. Singh Raman, P. Chakraborty Banerjee, D. E. Lobo, H. Gullapalli, M. Sumandasa, A. Kumar, L. Choudhary, R. Tkacz, P. M. Ajayan and M. Majumder, *Carbon*, 2012, **50**, 4040.
9. N. T. Kirkland, T. Schiller, N. Medhekar and N. Birbilis, *Corros. Sci.*, 2012, **56**, 1.
10. C.-H. Chang, T.-C. Huang, C.-W. Peng, T.-C. Yeh, H.-I. Lu, W.-I. Hung, C.-J. Weng, T.-I. Yang and J.-M. Yeh, *Carbon*, 2012, **50**, 5044.
11. A. S. Kousalya, A. Kumar, R. Paul, D. Zemlyanov and T. S. Fisher, *Corros. Sci.*, 2013, **69**, 5.
12. U. Khan, P. May, A. O'Neill, A. P. Bell, E. Boussac, A. Martin, J. Semple and J. N. Coleman, *Nanoscale*, 2013, **5**, 581.
13. F. Wackenhut, A. V. Failla and A. J. Meixner, *Phys. Chem. Chem. Phys.*, 2013, **15**, 5407.
14. Y. Cao, M. Zhu, P. Li, R. Zhang, X. Li, Q. Gong, K. Wang, M. Zhong, D. Wu, F. Lin and H. Zhu, *Phys. Chem. Chem. Phys.*, 2013, **15**, 19550.
15. D. S. L. Abergel and V. I. Fal'ko, *Phys. Rev. B*, 2007, **75**, 155430.
16. D. Li, M. B. Muller, S. Gilje, R. B. Kaner and G. G. Wallace, *Nat. Nanotechnol.*, 2008, **3**, 101.
17. U. Khan, A. O'Neill, H. Porwal, P. May, K. Nawaz and J. N. Coleman, *Carbon*, 2012, **50**, 470.
18. A. C. Ferrari, J. C. Meyer, V. Scardaci, C. Casiraghi, M. Lazzeri, F. Mauri, S. Piscanec, D. Jiang, K. S. Novoselov, S. Roth and A. K. Geim, *Phys. Rev. Lett.*, 2006, **97**, 187401.
19. Y. Hernandez, V. Nicolosi, M. Lotya, F. M. Blighe, Z. Sun, S. De, I. T. McGovern, B. Holland, M. Byrne, Y. K. Gun'Ko, J. J. Boland, P. Niraj, G. Duesberg, S. Krishnamurthy, R. Goodhue, J. Hutchison, V. Scardaci, A. C. Ferrari and J. N. Coleman, *Nat. Nanotechnol.*, 2008, **3**, 563.
20. U. Khan, A. O'Neill, M. Lotya, S. De and J. N. Coleman, *Small*, 2010, **6**, 864.
21. M. Lotya, P. J. King, U. Khan, S. De and J. N. Coleman, *ACS Nano*, 2010, **4**, 3155.
22. S. T. Huxtable, D. G. Cahill, S. Shenogin, L. Xue, R. Ozisik, P. Barone, M. Usrey, M. S. Strano, G. Siddons, M. Shim and P. Keblinski, *Nat. Mater.*, 2003, **2**, 731.
23. M. Moniruzzaman and K. I. Winey, *Macromolecules*, 2006, **39**, 5194.
24. L. Huang, C. Li, W. Yuan and G. Shi, *Nanoscale*, 2013, **5**, 3780.
25. J. M. D'Arcy, H. D. Tran, A. Z. Stieg, J. K. Gimzewski and R. B. Kaner, *Nanoscale*, 2012, **4**, 3075.

26. X.-H. Zhao, Z.-G. Shen, Y.-S. Xing and S.-L. Ma, *J. Phys. D: Appl. Phys.*, 2001, **34**, 2308.
27. M. Yi, W. Zhang, Z. Shen, X. Zhang, X. Zhao, Y. Zheng and S. Ma, *J. Nanopart. Res.*, 2013, **15**, 1811.
28. X. Wang, X. Zhao, M. Wang and Z. Shen, *Polym. Eng. Sci.*, 2007, **47**, 1156.
29. M. Wang, X. Zhao, Z. Shen, S. Ma and Y. Xing, *Polym. Degrad. Stab.*, 2004, **86**, 521.
30. M. Z. Hossain, J. E. Johns, K. H. Bevan, H. J. Karmel, Y. T. Liang, S. Yoshimoto, K. Mukai, T. Koitaya, J. Yoshinobu, M. Kawai, A. M. Lear, L. L. Kesmodel, S. L. Tait and M. C. Hersam, *Nat. Chem.*, 2012, **4**, 305.
31. N. A. Vinogradov, K. Schulte, M. L. Ng, A. Mikkelsen, E. Lundgren, N. Ma□rtensson and A. B. Preobrajenski, *J. Phys. Chem. C*, 2011, **115**, 9568.
32. A. Barinov, O. B. Malciog□lu, S. Fabris, T. Sun, L. Gregoratti, M. Dalmiglio and M. Kiskinova, *J. Phys. Chem. C*, 2009, **113**, 9009.
33. J. S. Bunch, S. S. Verbridge, J. S. Alden, A. M. van der Zande, J. M. Parpia, H. G. Craighead and P. L. McEuen, *Nano Lett.*, 2008, **8**, 2458.
34. O. Leenaerts, B. Partoens and F. M. Peeters, *Appl. Phys. Lett.*, 2008, **93**, 193107.
35. M. Topsakal, H. Şahin and S. Ciraci, *Phys. Rev. B*, 2012, **85**, 155445.
36. L. Rodriguez-Perez, M. A. Herranz and N. Martin, *Chem. Commun.*, 2013, **49**, 3721.
37. S. P. Surwade, Z. Li and H. Liu, *J. Phys. Chem. C*, 2012, **116**, 20600.
38. S. Fujii and T. Enoki, *J. Am. Chem. Soc.*, 2010, **132**, 10034.
39. J.-L. Li, K. Kudin, M. McAllister, R. Prud'homme, I. Aksay and R. Car, *Phys. Rev. Lett.*, 2006, **96**, 176101.
40. T. Sun and S. Fabris, *Nano Lett.*, 2012, **12**, 17.
41. X. Zhang, J. Xin and F. Ding, *Nanoscale*, 2013, **5**, 2556.
42. J. T. Paci, T. K. Minton and G. C. Schatz, *Acc. Chem. Res.*, 2012, **45**, 1973.